

Copper impairs the intestinal barrier integrity in Wilson disease

Adriana Fontes^{a,b,c}, Hannah Pierson^d, Joanna B. Bierła^e, Carola Eberhagen^a, Jennifer Kinschel^f, Banu Akdogan^a, Tamara Rieder^f, Judith Sailer^f, Quirin Reinold^f, Joanna Cielecka-Kuszyk^e, Sylwia Szymańska^e, Frauke Neff^g, Katja Steiger^h, Olga Seelbach^h, Andree Zibertⁱ, Hartmut H. Schmidtⁱ, Stefanie M. Hauck^j, Christine von Toerne^j, Bernhard Michalke^k, Jeremy D. Semrau^l, Ana M. DiSpirito^m, João Ramalho-Santos^{b,c,n}, Guido Kroemer^{o,p,q}, Roman Polishchuk^r, Anabela Marisa Azul^{b,n,s}, Alan DiSpirito^m, Piotr Socha^t, Svetlana Lutsenko^d, Hans Zischka^{a,f,*,1}

^a Institute of Molecular Toxicology and Pharmacology, Helmholtz Center Munich, German Research Center for Environmental Health, Neuherberg, Germany

^b CNC-Center for Neuroscience and Cell Biology, University of Coimbra, Coimbra, Portugal

^c DCV-Department of Life Sciences, Faculty of Sciences and Technology of the University of Coimbra, Coimbra, Portugal

^d Department of Physiology, Johns Hopkins Medical Institutes, Baltimore, MD, USA

^e Department of Pathomorphology, Children's Memorial Health Institute, Al. Dzieci Polskich 20, 04-730 Warsaw, Poland

^f Technical University Munich, Institute of Toxicology and Environmental Hygiene, Munich, Germany

^g Munich Clinic Harlaching, Munich, Germany

^h Comparative Experimental Pathology Department, Institute for General Pathology and Pathological Anatomy, Technical University of Munich (TUM), Germany

ⁱ Medizinische Klinik B für Gastroenterologie und Hepatologie, Universitätsklinikum Münster, Münster, Germany

^j Research Unit Protein Science, Helmholtz Center Munich, German Research Center for Environmental Health GmbH, Munich, Germany

^k Research Unit Analytical BioGeoChemistry, Helmholtz Center Munich, German Research Center for Environmental Health, Neuherberg, Germany

^l Department of Civil and Environmental Engineering, University of Michigan, Ann Arbor, MI, 48109-2125, USA

^m Roy J. Carver Department of Biochemistry, Biophysics and Molecular Biology, Iowa State University, Ames, USA

ⁿ CIBB-Center for Innovative Biomedicine and Biotechnology (CIBB), University of Coimbra, Coimbra, Portugal

^o Centre de Recherche des Cordeliers, Equipe labellisée par la Ligue contre le cancer, Université Paris Cité, Sorbonne Université, Inserm U1138, Institut Universitaire de France, Paris, France

^p Metabolomics and Cell Biology Platforms, Institut Gustave Roussy, Villejuif, France

^q Institut du Cancer Paris CARPEM, Department of Biology, Hôpital Européen Georges Pompidou, AP-, HP, Paris, France

^r Telethon Institute of Genetics and Medicine, 80078 Pozzuoli, Italy

^s IIIUC-Institute for Interdisciplinary Research, University of Coimbra, Coimbra, Portugal

^t Department of Gastroenterology, Hepatology, Nutritional Disorders and Pediatrics, Children's Memorial Health Institute, Al. Dzieci Polskich 20, 04-730 Warsaw, Poland

ARTICLE INFO

Keywords:

Intestine
Copper
Mitochondria

ABSTRACT

In Wilson disease (WD), liver copper (Cu) excess, caused by mutations in the ATPase Cu transporting beta (ATP7B), has been extensively studied. In contrast, in the gastrointestinal tract, responsible for dietary Cu uptake, ATP7B malfunction is poorly explored. We therefore investigated gut biopsies from WD patients and

Abbreviations: ALT, alanine aminotransferase; AST, aspartate aminotransferase; ATP7A, ATPase copper transporting alpha; ATP7B, ATPase copper transporting beta; BSA, bovine serum albumin; Caco-2, Cancer coli-2; Caco-2 KO, Caco-2 ATP7B knockout cells; Caco-2 WT, Caco-2 wild-type cells; CCCP, carbonyl cyanide *m*-chlorophenylhydrazine; Ccl, capacitance; CTR1/2, high affinity copper uptake protein 1/2; Cu, copper; DMEM, Dulbecco's modified eagle medium; DPBS, Dulbecco's phosphate buffered saline; ECAR, extracellular acidification rate; FBS, fetal bovine serum; FDR, false discovery rate; GI, gastrointestinal; H&E, hematoxylin and eosin; ICP-OES, inductively coupled plasma optical emission spectroscopy; LC-MSMS, liquid chromatography with tandem mass spectrometry; MALT, mucosal associated lymphatic tissue; MB, methanobactin; MEM, minimum essential medium; MT, metallothioneins; NEAA, non-essential amino acids; OCR, oxygen consumption rate; OCT, Optimal cutting temperature; RIPA, radio-immunoprecipitation assay; TEER, transepithelial electrical resistance; TG, triglycerides; TJ, tight-junctions; WD, Wilson disease; TJP1/ZO-1, tight-junction protein 1/zonula occludens 1.

* Corresponding author at: Institute of Molecular Toxicology and Pharmacology, Helmholtz Center Munich, German Research Center for Environmental Health, D-85764 Neuherberg, Germany.

E-mail address: hans.zischka@helmholtz-munich.de (H. Zischka).

¹ Technical University Munich, School of Medicine, Institute of Toxicology and Environmental Hygiene, Biedersteiner Strasse 29, D-80802 Munich, Germany.

<https://doi.org/10.1016/j.metabol.2024.155973>

Received 17 February 2024; Accepted 5 July 2024

Available online 8 July 2024

0026-0495/© 2024 The Authors. Published by Elsevier Inc. This is an open access article under the CC BY-NC license (<http://creativecommons.org/licenses/by-nc/4.0/>).

Wilson disease
Methanobactin

compared intestines from two rodent WD models and from human *ATP7B* knock-out intestinal cells to their respective wild-type controls.

We observed gastrointestinal (GI) inflammation in patients, rats and mice lacking *ATP7B*. Mitochondrial alterations and increased intestinal leakage were observed in WD rats, *Atp7b*^{-/-} mice and human *ATP7B* KO Caco-2 cells. Proteome analyses of intestinal WD homogenates revealed profound alterations of energy and lipid metabolism. The intestinal damage in WD animals and human *ATP7B* KO cells did not correlate with absolute Cu elevations, but likely reflects intracellular Cu mislocalization. Importantly, Cu depletion by the high-affinity Cu chelator methanobactin (MB) restored enterocyte mitochondria, epithelial integrity, and resolved gut inflammation in WD rats and human WD enterocytes, plausibly via autophagy-related mechanisms.

Thus, we report here before largely unrecognized intestinal damage in WD, occurring early on and comprising metabolic and structural tissue damage, mitochondrial dysfunction, and compromised intestinal barrier integrity and inflammation, that can be resolved by high-affinity Cu chelation treatment.

1. Introduction

In Wilson disease (WD), mutations in *ATP7B* impair biliary Cu excretion, leading to hepatic Cu overload [1,2]. If left untreated, WD is a lethal condition, mainly due to devastating Cu effects on hepatocyte mitochondria and lysosomes [3–8]. Consequently, current therapies aim to establish Cu homeostasis by either elevating Cu excretion or reducing its dietary uptake [9,10]. Hundreds of loss-of-function mutations in *ATP7B* have been identified [11]. However, a major issue in WD is the lack of a clear genotype-phenotype relation, leaving patients and clinicians with profound uncertainties of how the disease will develop or how a chosen treatment will work [1]. Indeed, beyond hepatic *ATP7B* malfunction, additional factors that include Cu exposure but also lifestyle factors contribute to WD progression [12,13].

We have recently reported severe aggravation of the disease in WD rats when put on a high-caloric diet [13]. This directed our attention to the GI-tract in WD, as systemic Cu uptake primarily occurs at the level of the small intestine [14]. In fact, Weiss and colleagues showed that the intestinal expression of *ATP7B* may act as an additional regulatory mechanism for Cu absorption alongside the high affinity copper uptake protein 1 (CTR1) and ATPase copper transporting alpha (*ATP7A*) [15]. Thereto, Pierson and co-workers [16] demonstrated that *ATP7B* was abundant in enterocytes from duodenal crypts, mostly located in intracellular vesicles, and that its levels and subcellular localization were regulated by changes in Cu. These observations led to the suggestion that intestinal *ATP7B* participates in vesicular Cu storage [16]. Accordingly, the gut from WD (*Atp7b*^{-/-}) mice contains less Cu than the gut from wild type (WT) control mice, which is very different from what is seen in the liver. Nonetheless, enterocytes from WD mice exhibit mitochondrial structure impairments and lipid accumulation indicating changes in dietary fat processing [16]. A disturbed lipid metabolism was also reported for human colon carcinoma Caco-2 cells lacking *ATP7B* (which can be considered a human WD enterocyte model). Such cells are sensitive to Cu toxicity and exhibit reduced triglyceride (TG) storage and secretion [17].

Abdominal pain is a clinical symptom in up to 40 % of WD patients at diagnosis [9]. Moreover, ulcerative colitis has been reported as a comorbidity in WD patients, including two 8-year-old [18] and 17-year-old females [19] and a 24-year-old male [20]. In addition, alterations in the composition of the gut microbiota were reported for WD patients, in comparison to healthy controls [21,22]. In a recent study by Sarode and coworkers, systemic *Atp7b* KO mice exhibited reduced gut microbiota diversity, with changes in phyla and genera that correlate with liver disease and fatty liver, and altered lipidomic profiles [23]. Finally, GI problems, such as gastric irritation (gastritis, erosions and ulcers), appear in up to 30 % of patients treated by zinc salts [24–26]. The rationale for therapeutic zinc salts is to lower systemic Cu by elevating intestinal metallothionein, therefore promoting its sequestration and removal via enterocyte desquamation [24,27–29]. However, it appears possible that WD predisposes patients to such GI toxicity.

Driven by these premises, we investigated two rodent WD models and an in vitro model of human WD enterocytes for possible disease-

relevant alterations. Beyond mitochondrial alterations, we observed an impairment of enterocyte barrier integrity that is clearly pro-inflammatory. High-affinity chelation of Cu could reverse these effects.

2. Results

2.1. Intestinal damage is present in Wilson disease patients

In two WD patients (WDP – 1 and WDP – 2, Fig. 1), intestinal inflammation was observed upon histologic analysis. The first patient (WDP-1) was diagnosed with WD at the age of 7.5 years, after manifesting increased alanine aminotransferase (ALT)/AST values from the age of 4. The liver biopsy showed intermediate fibrosis with mild steatosis and inflammation. The 24-h Cu excretion was 108 µg, and ceruloplasmin 0.09 g/L. Diagnosis was molecularly confirmed (H1069Q and W779* mutations in *ATP7B*). The patient started treatment with DPA which improved the liver damage (ALT values went down, nonetheless remaining slightly elevated until the age of 12). At the age of 15, the patient had occasional abdominal pain and increased IgA antibodies against tissue transglutaminase (46 U/mL). Consequently, endoscopic examination was performed, following the recommendations of the European Society for Paediatric Gastroenterology, Hepatology and Nutrition (ESPGHAN). The second patient (WDP – 2) was diagnosed with Crohn's disease at 15 years of age, with suspected autoimmune hepatitis due to increased circulating transaminases. A liver biopsy performed at the same age showed moderate fibrosis, inflammation, and steatosis (30 % of hepatocytes). The 24-h Cu excretion was 97 µg, ceruloplasmin 0.08 g/L and liver Cu content 1599 µg/g. Treatment with DPA was initiated, together with treatment for Crohn's disease. Histopathological examination of duodenal biopsies of WDP-1 revealed flattened villi and widened crypts (WDP-1, Fig. 1A, C). In agreement, histopathological analysis of the ileum of the WDP – 2 revealed erosions, crypt distortions, and infiltration of the lamina propria by lymphocytes and eosinophils (WDP – 2, Fig. 1A). In both patients, the small intestine architecture was visibly changed in comparison to the control patients (C-1, Fig. 1A; C – 2, Fig. 1B). Furthermore, an increased intraepithelial lymphocytosis up to 80 CD3⁺/100 epithelial cells (Fig. 1C), which corresponds to stage IIIB villous atrophy on the Marsh scale was observed in WDP-1, in comparison to a control patient (Fig. 1B-C). The large intestine architecture of WDP-1 and 2 was not as altered as the small intestine. Nonetheless, in WDP-1, altered crypts were also observed in comparison to the control patient (C-1, Fig. 1A).

2.2. Rodent models replicate the intestinal damage observed in Wilson disease patients

To investigate whether intestinal damage occurs in the context of WD, we analysed the duodenum and colon from LPP *Atp7b*^{-/-} rats (WD rats) and *Atp7b*^{-/-} WD-mice using H&E staining. The small intestine of WD rats showed lymphocyte infiltrations and detachments of the lamina propria, while the duodenum of *Atp7b*^{-/-} mice exhibited submucosal inflammation (Fig. 1A). In the colon, submucosal inflammation with

cryptic distortions was found in both WD rats and *Atp7b*^{-/-} mice (Fig. 1A). Of note, in WD rats, inflammation and structural alterations in the small intestine were evident even before the onset of manifest hepatic disease. Up to an age of ~90 days, WD rats appear healthy, although they later develop laboratory signs of liver damage such as elevated circulating transaminases and total bilirubin (AST > 200 U/L,

T-Bili >0.5 mg/dL). Untreated, WD rats die around an age of 120 days [30–32]. The determination of Cu levels in still healthy and diseased WD rats further revealed a significantly elevation of Cu in the duodenum of diseased animals in the latter ($P = 0.0043$) (Fig. 2A). Intriguingly, and in agreement with a prior report on *Atp7b*^{-/-} mice [16], still healthy WD rats had even lower intestinal Cu levels than controls (Fig. 2A).

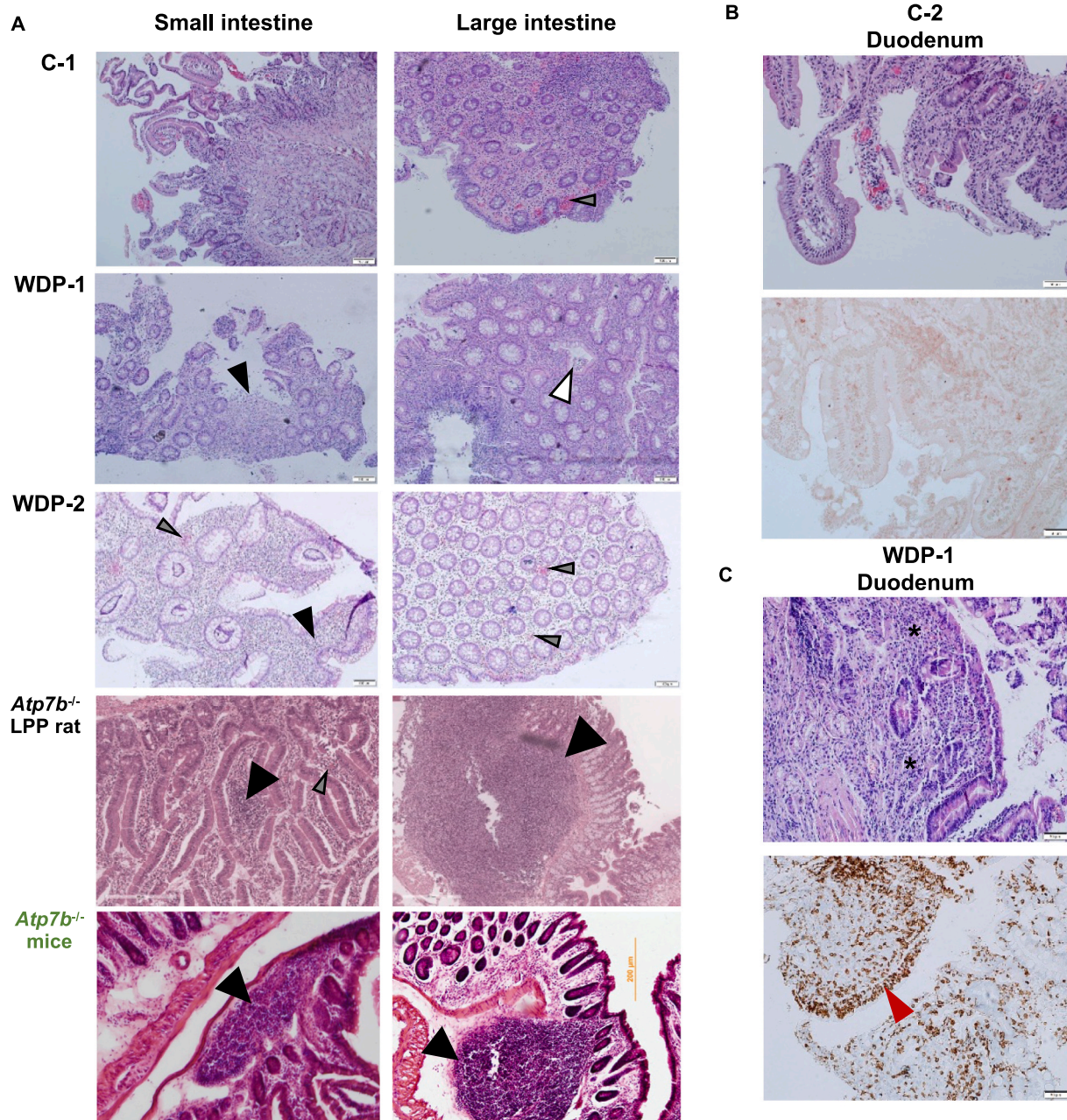


Fig. 1. Intestinal damage in Wilson disease (WD). (A) Left panels: H&E-stained small intestine of two WD patients (WDP-1 and WDP-2) show erosions on the surface and changes in the lamina propria due to lymphocyte infiltrations (black arrow, scale bar: 100 μ m), together with eosinophils infiltration (grey arrows). The same features are largely absent in the sample from the control patient (C-1) (scale bar: 100 μ m). In agreement, the small intestine of WD rats also presents increased mucosal infiltration, mainly lymphocytic, frequently in follicular arrangement (black arrows), with eosinophils infiltration (grey arrows) (scale bar: 200 μ m). In *Atp7b*^{-/-} mice duodenal tissue, a strong submucosal inflammation is observed (black arrow, scale bar: 200 μ m). Right panels: In the large intestine of WD patients, H&E staining reveals a mild crypt architecture disorder, nodular reaction in the lamina propria (white arrow), mild lymphocytic-plasma inflammation and erosions, with eosinophils infiltration (grey arrow) (scale bar: 100 μ m). In the control, infiltration of eosinophils is also observed (grey arrow). However, the crypt architecture is not changed in comparison to WDP-1 (scale bar: 100 μ m). Submucosal infiltration of immune cells is prominent in the colon of WD rats (scale bar: 300 μ m), and in *Atp7b*^{-/-} mice (57 weeks old) (black arrows), in which the crypts appeared stunted and widely spaced with mucosal associated lymphatic tissue (MALT, scale bar: 200 μ m). (B and C) Histopathological examination of duodenal samples from WDP-1, (extrabulbar areas), show flattened villous part and widening of crypts (black asterisks) and increased intraepithelial lymphocytosis up to 80 CD3/100 epithelial cells (red arrow). In the control sample (C-2), no visible changes in the villi and crypts are observed, together with the absence of intraepithelial lymphocytosis (no CD3 positive staining). (For interpretation of the references to colour in this figure legend, the reader is referred to the web version of this article.)

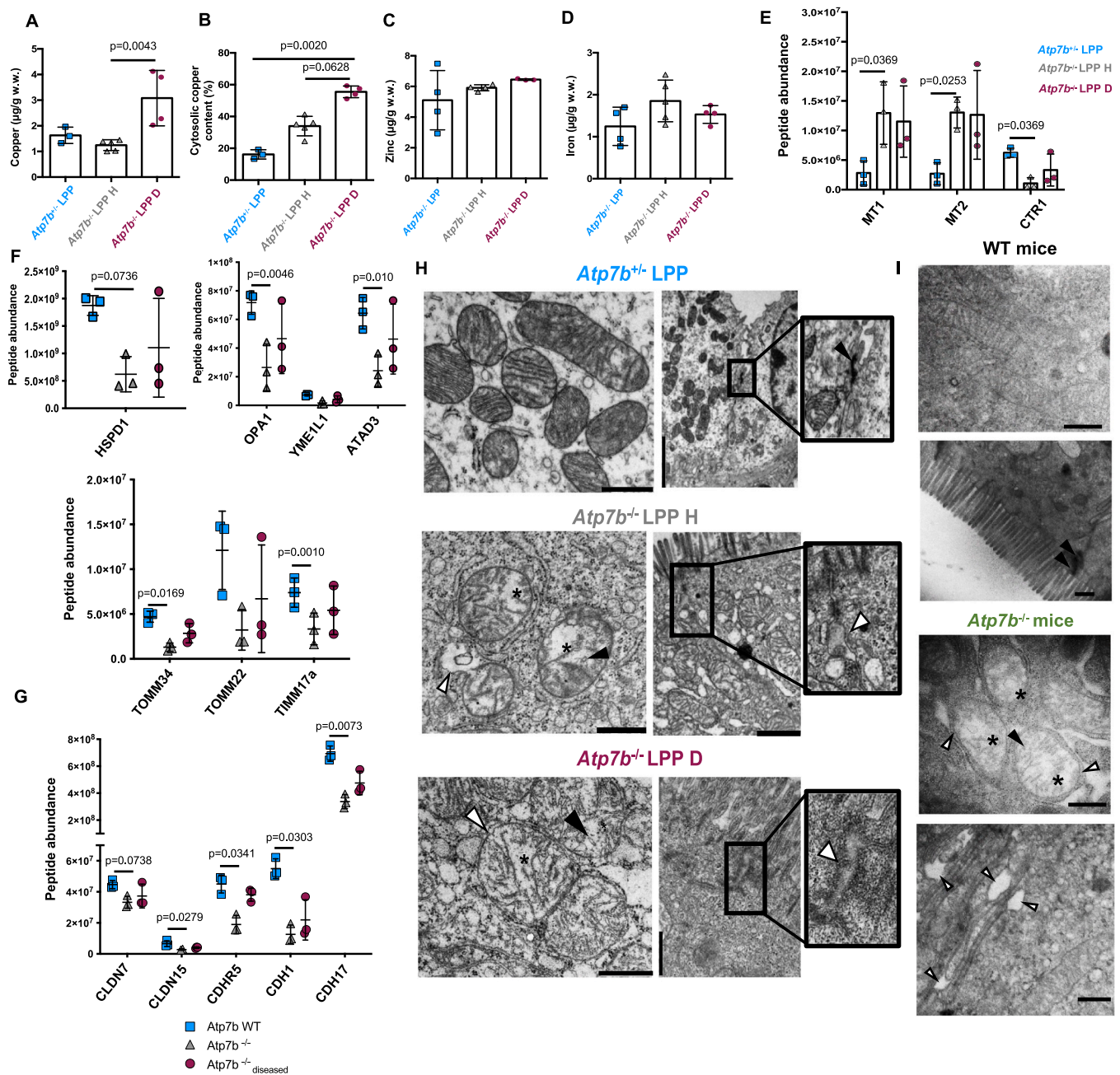


Fig. 2. Copper content, mitochondrial alterations, and disrupted cell-cell barrier in the small intestine of WD rodents. **(A)** Increased copper levels in the small intestine of diseased WD rats (D) are measured in comparison to controls and still healthy (H) animals. **(B)** Cytosolic copper content (in % of total tissue copper content) progressively and significantly increased from still healthy to diseased WD rats vs. controls. **(C)** No significant changes are observed for zinc levels or **(D)** iron levels. Proteome comparisons of the small intestine (predominantly duodenum) reveal a significant increase in **(E)** Metallothionein 1 and 2 (MT1, MT2), but a CTR1 decrease in WD vs. control rats, **(F)** a significant decrease in Hspd, Opa1 and Atad3, in still healthy WD rats vs control, and a significant decrease in Tomm34 and Timm17a. A decreased protein abundance was observed for Yme111 and Tomm22. **(G)** The protein abundance of proteins related to the epithelial barrier integrity was significantly decreased, namely for Cldn7 and 15, Cdh5, 1 and 17. **(H)** Left panel: electron micrographs of duodenum from WD rats (scale bar: 500 nm) present mitochondrial structure alterations with cristae disorganization (black arrows), loss of electron dense matrices (black asterisk) and outer mitochondria membrane irregularities (white arrows). Right panel: WD rats present with less dense TJ-like areas with widening of the intercellular adhesion spaces (white arrows) (scale bar: 1000 nm and 500 nm for LPP D), in contrast to electron-dense high-protein TJ area in controls (black arrow). **(I)** In contrast to an elongated tubular morphology in controls (WT), small intestine *Atp7b*^{-/-} mice mitochondria have a roundish morphology, with depleted and unorganized cristae (black arrow), a loss of electron dense matrices (black asterisk) and detachment of the outer mitochondria membrane (white arrows) (scale bar: 500 nm). In WT mice duodenal epithelium, the presence of brush borders with TJ-protein dense areas (black arrows) is pronounced, while in *Atp7b*^{-/-} mice, lateral membranes appear “loose” with widenings between neighboring epithelial cells (white arrows) (scale bar: 500 nm). Data are the mean ± SD of N = 3–5 (A–D) or N = 3 (E–G). One-way analysis of variance (Kruskal-Wallis), followed by Dunn’s multiple comparisons test. ATAD3, ATPase family AAA domain-containing protein 3; CDH1, Cadherin 1; CDH5, Cadherin 5; CDH17, Cadherin 17; CLDN7, Claudin-7; CLDN15, Claudin 15; HSPD1, 60 kDa heat shock protein; OPA1, Dynamin-like 120 kDa protein; TIMM17a, Mitochondrial import inner membrane translocase subunit Tim17A; TOMM22, Mitochondrial import receptor subunit TOM22 homolog; TOMM34, Mitochondrial import receptor subunit TOM34; YME111, ATP-dependent zinc metalloprotease.

However, although total Cu was low in still healthy WD rats, their relative cytosolic Cu content was elevated compared to controls, and this percentage further increased significantly in diseased animals ($P = 0.0020$) (Fig. 2B), indicating that Cu is progressively mislocalized in cells from the WD rat intestine (see below). No significant alterations were observed for zinc (Fig. 2C), or iron levels (Fig. 2D). The increased relative cytosolic Cu content correlated with signs of cell stress such as significantly elevated metallothioneins (MT1 and MT2) ($P = 0.0369$ and $P = 0.0253$, respectively), but also reduced expression of the Cu uptake transporter CTR1 ($P = 0.0369$) (Fig. 2E).

2.3. Mitochondrial structures and barrier integrity are altered in enterocytes from rodents with Wilson disease

Liver mitochondria are key targets of elevated Cu^{2+} in WD [3–5]. We therefore analysed mitochondrial alterations in the guts from rats and mice lacking ATP7B. Compared to controls, a proteome analysis from the small intestine tissue of still healthy and diseased WD rats revealed a decreased abundance of the mitochondrial heat shock protein 60 (Hspd1) in still healthy WD rats, along with essential proteins for mitochondria organization and structure such as mitochondrial dynamin like GTPase (OPA1) ($P = 0.0046$), ATP-dependent zinc metalloprotease YME1L1 (YME1L1) and ATPase Family AAA Domain containing 3 A (ATAD3) ($P = 0.010$) (Fig. 2F). Moreover, mitochondria protein import system is compromised as observed by the decreased abundance of TOMM34 ($P = 0.0169$), TOMM22 and TIMM17a ($P = 0.0010$) (Fig. 2F). In direct correlation, mitochondrial structures were altered in both still healthy and diseased WD rat enterocytes, i.e., these organelles were enlarged, had electron-translucent matrices, membrane deformations, and widened vesicular cristae (Fig. 2H). Highly similar features were observed in mitochondria from duodenal tissue of *Atp7b*^{-/-} mice (Fig. 2I). Importantly, these enterocyte-specific mitochondrial alterations profoundly differed from those encountered in WD livers, which are characterized by intramitochondrial contractions (not dilations) and abnormally electron-dense (not electron-translucent) matrices (Supplementary Fig. 1). Depletion of several claudins and cadherins ($0.0073 < P < 0.0738$) (Fig. 2G), indicated deficits in cell-cell contacts in the duodenum of WD rats. This is in accord with transmission electron micrographs revealing less electron-dense desmosomes (indicating reduced protein content) and widening of enterocyte tight junctions (TJ) in both WD rats and *Atp7b*^{-/-} mice (Fig. 2H, I). Therefore, alterations in the small intestine metabolism are paralleled by a potential increase in gut leakiness in both WD rats and mice. Furthermore, from the tissue proteome analysis, a potential metabolic shift towards glycolysis was observed, with a significant increased abundance of hexokinase-1, together with alterations in the expression of proteins directly correlated with digestion and transmembrane transport in the gut (Table 1). Moreover, the small intestinal proteomes of still healthy and diseased WD rats vs. controls revealed, among others, a significant decreased abundance of proteins for lipoprotein assembly, remodelling and clearing (Supplementary Table 1). As this essential enterocytic function is reportedly impaired in *Atp7b*^{-/-} mice [16,23], these findings support a disbalance in intestinal lipid metabolism in WD rats.

2.4. Mitochondrial damage and impaired barrier formation in a human Wilson disease enterocyte model

To demonstrate the causal link between ATP7B deficiency and enterocytic alterations, Caco-2 cells carrying an ATP7B knockout (Caco-2 KO³³, Supplementary Fig. 2A) were compared to their WT controls. Comparable to the aforementioned observations in ATP7B-deficient rodents, mitochondrial structure deficits were apparent in Caco-2 KO cells, but not in WT control cells (Fig. 3A). The organelles appeared bigger with electron-translucent mitochondrial matrices and rarefied cristae. Such structural deficits were aggravated, in both cell lines, by a short-term challenge with 100 μM CuCl_2 (Fig. 3A). To

quantify the changes in mitochondrial structures, a four-stage scoring system was applied. Thereat, Stage I indicated mitochondria with a distinguishable network of cristae, no visible alterations in the outer or inner membrane and an electron-dense matrix, and Stage IV indicated mitochondria with no distinguishable network of cristae, damage to the inner membrane and visible swelling, whereas Stages II and III presented intermediate changes. Untreated Caco-2 KO cells had a significant ($P = 0.0235$) decrease of Stage I mitochondria, with an increase in Stage IV ($P = 0.0542$) (Fig. 3B, C), in comparison to untreated Caco-2 WT cells. Copper treatment did not significantly alter mitochondrial structures in Caco-2 KO cells, however, WT cells had a significant increase in Stage IV mitochondria upon treatment ($P = 0.0315$) (Fig. 3B, C). These structural impairments were accompanied by functional deficits, as mitochondria of Caco-2 KO cells exhibited lower maximal respiratory capacities (MR) than WT cells, and a significant decrease in spare respiratory capacity upon Cu treatment ($P = 0.0224$) (SRC, Fig. 3D). Already at basal conditions, i.e., in the absence of Cu supplementation, oxidative phosphorylation was at maximum in Caco-2 KO cells. The addition of Cu further decreased the mitochondrial metabolic potential (Fig. 3E). As in WD rats, proteome comparisons of Caco-2 WT vs. KO cells validated the mitochondrial dysfunction of KO cells (Supplementary Fig. 2B, Supplementary Table 2). The deficit in oxidative phosphorylation of Caco-2 KO cells was counterbalanced by enhanced glycolytic activity, as indicated by a significant extracellular acidification rate ($P < 0.0001$) (Fig. 3F), giving rise to a reduction of the pH of the culture medium (Supplementary Fig. 2C), as well as by a pronounced overabundance of hexokinase-1 (Supplementary Table 2).

As mitochondrial dysfunction has been repeatedly reported to impair cell-cell contacts [34–36], which indeed were reduced in the intestines of both WD animal models (Fig. 2), we comparatively analysed barrier formation by Caco-2 KO and WT cells. Upon cultivation for 21 days, Caco-2 cells progressively form cellular monolayers that resemble intestinal barriers. Their progressive intercellular connection via TJ can be followed biophysically by assessing trans-epithelial electrical resistance (TEER) that steadily increases (Supplementary Fig. 3A). In addition, the capacitance of such cellular monolayers is proportional to the cell surface area, thereby providing further information, e.g., on the number and length of villi [37].

Over a period of 21 days, Caco-2 KO monolayers were consistently less tight than controls (Fig. 4A), although KO monolayers exhibited a comparatively higher capacitance (Supplementary Fig. 3B, C), likely due to longer villi (Supplementary Fig. 3D). A significant lower TEER was observed for the Caco-2 KO cells at 14 days ($P = 0.0038$) and 16 days ($P = 0.0057$) (Fig. 1A). In WD rats and mice, electron micrographs revealed impaired enterocytic contact sites (Fig. 2H, I). Such widening of the intercellular space was also observed in Caco-2 KO monolayers compared to WT controls (Fig. 4C), together with a significant lower abundance of key proteins in the maintenance of the barrier integrity such as occluding ($P = 0.0022$) and claudin-4 ($P = 0.0022$) (Fig. 4B). Moreover, immunofluorescence staining revealed a more disorganized pattern of the TJ¹ protein occludin, and a lower abundance of the tight junction protein 1 (TJP-1) in Caco-2 KO cells, in comparison to control (Fig. 4D). Thus, in mice, rats and human Caco-2 cells lacking ATP7B, similar mitochondrial deficits and impaired cell-cell contact formations were concordantly detected.

2.5. Copper causes impairments in the human Wilson disease enterocyte model

In liver, ATP7B malfunction causes excess Cu accumulation. However, in the WD rat intestine, such Cu accumulation was only measured upon manifestation of overt liver disease (Fig. 2A). Nevertheless, mitochondrial dysfunction and impaired barrier integrity (and an associated gut inflammation) were seen in WD rats before they developed manifest liver pathology as well as in human Caco-2 KO enterocytes cultured without extra Cu supplementation. This raises the question whether Cu

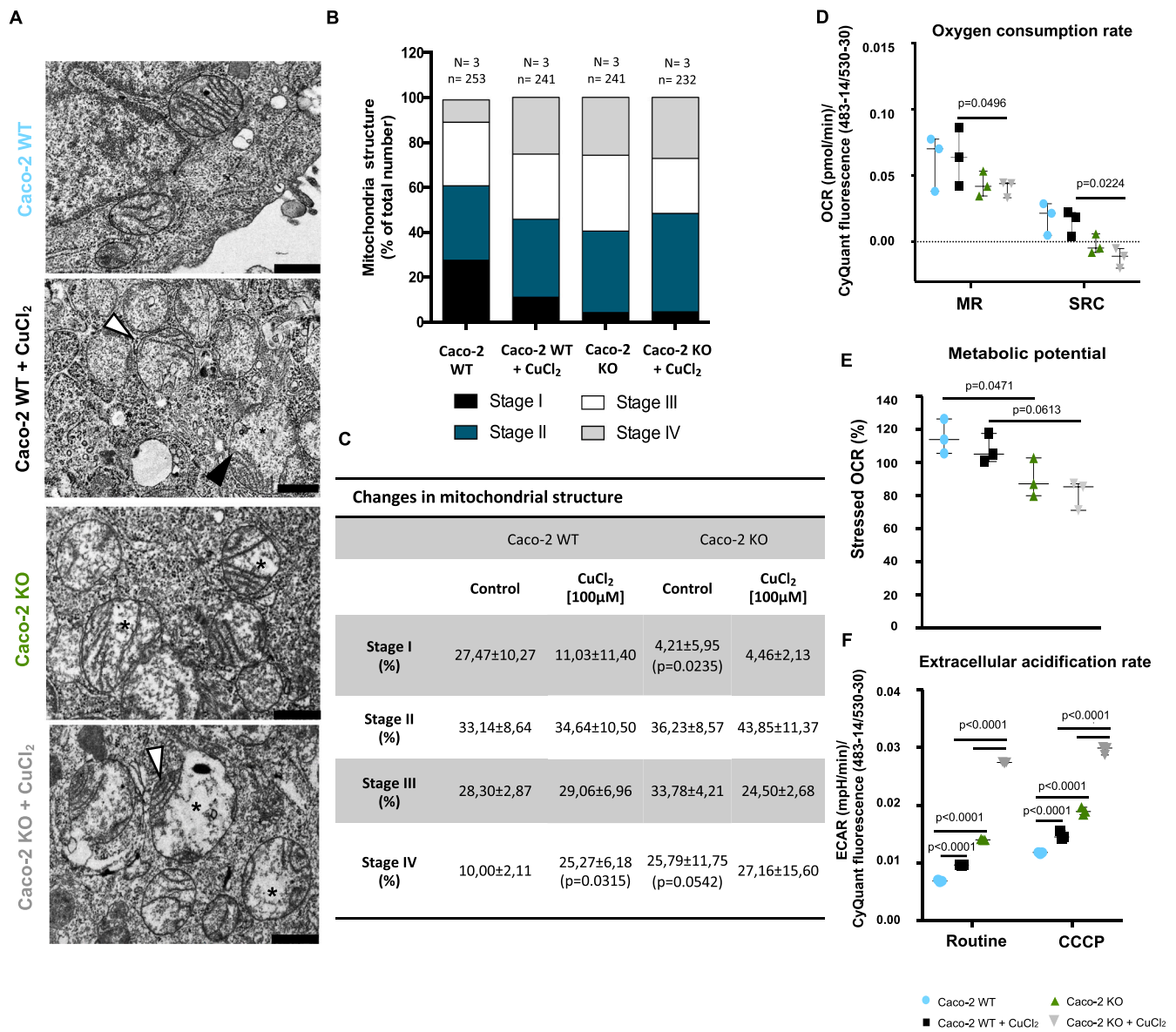


Fig. 3. Structural and functional mitochondrial deficits in a human WD enterocyte model. **(A)** Mitochondrial structure alterations in non-differentiated Caco-2 *ATP7B* KO cells (scale bar: 500 nm) with electron translucent matrices (black asterisks) and disorganized cristae (white arrows). Both features aggravate upon additional copper treatment (100 μM CuCl₂) in KO, as well as control cells. **(B, C)** Mitochondria structure is significantly altered in Caco-2 *ATP7B* KO cells in comparison to WT cells, and in WT cells treated with Cu. In *ATP7B* KO cells is observed a significant decrease in Stage I mitochondria with an increase in Stage IV mitochondria. Upon Cu treatment, it is observed a significant increase in Stage IV mitochondria in the WT cells. Stage I indicates mitochondria with a distinguishable network of cristae, no visible alterations in the outer or inner membrane and an electron-dense matrix, and Stage IV indicates mitochondria with no distinguishable network of cristae, damage to the inner membrane and visible swelling, whereas Stages II and III presented intermediate changes. **(D)** Decreased maximum mitochondrial respiratory capacity (MR) and spare respiratory capacity (SRC) of KO vs control cells, resulting **(E)** in a decreased metabolic potential (CCCP linked Oxygen consumption rate (OCR)/Baseline OCR x 100) of the KO cells. **(F)** The extracellular acidification rate (ECAR), a glycolytic activity marker, is significantly higher in KO vs. WT cells and further increases upon copper treatment. Data are the mean ± SD of N = 3, n = 232–253 (B,C) or N = 3, n = 3 (D–F). One-way analysis of variance (Kruskal-Wallis), followed by Dunn's multiple comparisons test (E), or Two-way analysis of variance followed by Tukey's multiple comparisons test (C, D, F).

is truly responsible for the perturbations observed in *ATP7B*-deficient enterocytes. Upon Cu-treatment, a significant increase in Cu levels was observed for WT and KO cells, when compared to their respective untreated controls ($P = 0.0161$ and $P = 0,0020$, respectively) (Fig. 5A). However, no significant differences in Cu were observed between whole cell extracts of Caco-2 KO and WT cells, neither at basal conditions nor upon additional Cu-treatment (Fig. 5A). For zinc and iron, a significant increase was observed in the Caco-2 KO cells upon Cu-treatment ($P = 0.0069$ and $P = 0.0279$, respectively) (Fig. 5B, C). Yet, upon Cu treatment followed by cellular sub-fractionation, a different intracellular Cu

distribution in Caco-2 KO vs WT cells became apparent (Fig. 7G). While the 800 g (containing cell debris and nuclei) and the 10.000 g fraction (containing mitochondria) had a less pronounced increase upon Cu-addition, the opposite (i.e., a higher Cu burden in Caco-2 KO vs WT cells) was observed for the 100.000 g (vesicular fraction) ($P = 0.0154$) and the cytosolic supernatant. This latter result agrees with the finding of a relatively increased cytosolic Cu content in WD vs. control rat intestines (Fig. 2B). Thus, *ATP7B* malfunction in WD enterocytes does not lead to overall excess Cu, but to distinct intracellular copper routing, with more Cu appearing in cytosol and vesicular compartments.

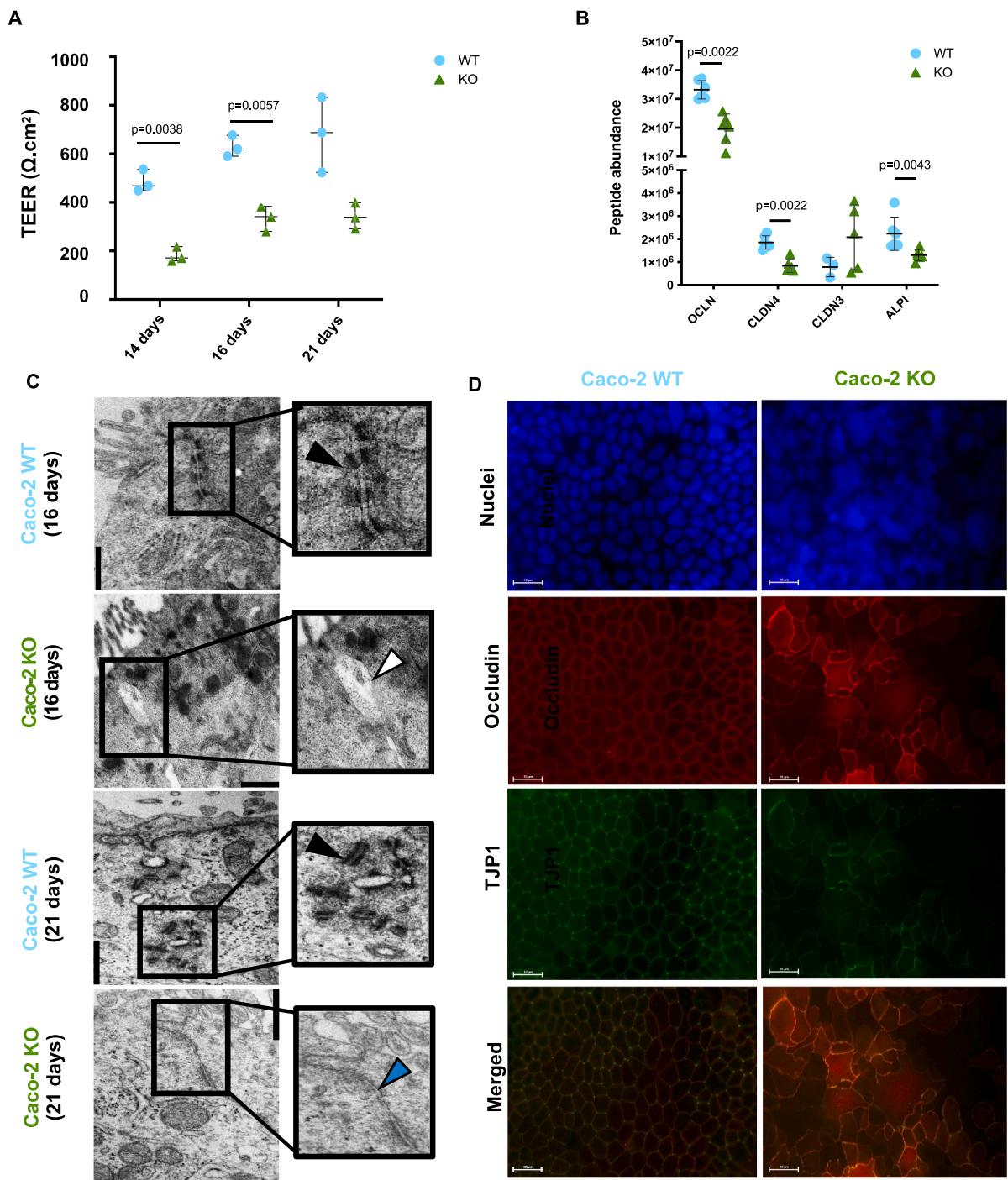


Fig. 4. Impaired cell-cell contacts in a human WD enterocyte model. **(A)** Caco-2 *ATP7B* KO monolayers have a consistently lower trans epithelial electrical resistance (TEER) in comparison to WT cells. **(B)** Proteome analysis revealed a significant decrease in OCLN, CLDN4 and ALPI abundance in KO cells vs control. **(C)** Electron micrographs of Caco-2 cell monolayers differentiated for 16 or 21 days (Scale bars: 1000 nm/500 nm). At 16 days of differentiation KO monolayers have widened intercellular spaces (white arrow). In contrast to protein dense desmosome-like structures in Caco-2 WT monolayers (black arrows), such mature structures are missing in Caco-2 KO cells, even after 21 days of differentiation (blue arrow). **(D)** Immunocytochemistry staining against occludin and the tight junction protein 1 (TJP1), demonstrates a regular cellular monolayer in Caco-2 WT but not in KO cells (scale bars: 10 μm). Data are the mean ± SD of N = 3 (A, B). Two-way analysis of variance followed by Sidak's multiple comparisons test (A), or Mann-Whitney test for 2-group data comparison (B). ALPI, alkaline phosphatase; CLDN3, claudin 3; CLDN4, claudin 4; OCLN, occludin. (For interpretation of the references to colour in this figure legend, the reader is referred to the web version of this article.)

While the molecular mechanisms of such Cu mislocalization must await future studies, it appears that the *ATP7B* deficiency, associated subcellular redistribution Cu has functional consequence. Three distinct cellular toxicity assays concordantly revealed a significant higher vulnerability of KO compared to WT cells to increasing extracellular Cu concentrations (Fig. 5D–F).

To further demonstrate that adverse Cu effects are already present at basal levels, i.e., in the absence of added Cu, we Cu-depleted differentiated Caco-2 KO cells by incubation with the high-affinity Cu chelator MB [30,31], from day 7 until day 21. Methanobactin strongly reduced the cellular Cu ($P = 0.0078$) (but not zinc or iron) content (Fig. 6A). Even short-term (24 h) treatment of Caco-2 KO cells with MB

Table 1

Atp7b knockout induces changes in the abundance of proteins directly linked to intestinal homeostasis in WD rats.

Symbol	Description	Abundance ratio (<i>Atp7b</i> ^{-/-} / <i>Atp7b</i> WT)	Abundance ratio (<i>Atp7b</i> ^{-/-} diseased/ <i>Atp7b</i> WT)	Cellular localization
Energy metabolism				
G6pc3	Glucose-6-phosphatase 3	0,28**	0,66	ER
Hk1	Hexokinase-1	1,75*	1,21	Cytoplasm, Mitochondrion
Pea15	Astrocytic phosphoprotein PEA-15	0,63	0,36****	Cytoplasm
Stxbp5	Syntaxin-binding protein 5	0,37*	0,84	Cell junction, Cell membrane, Cytoplasm
Pklr	Pyruvate kinase PKLR	0,51*	0,53***	Cell membrane, Cytosol
Myo1c	Unconventional myosin-1c	1,77*	1,36	Cell membrane, Cytoplasm
Aqp3	Aquaporin-3	0,38*	0,73	Basolateral cell membrane, Cell membrane, Cytoplasm,
Aqp7	Aquaporin-7	0,25**	0,52*	Cytoplasmic vesicle, Lipid droplet
Calm3	Calmodulin-3	0,56*	0,97	Cytoskeleton
Digestion and absorption/Transmembrane transport				
Cel	Bile salt-activated lipase	4,40****	2,74****	Secreted
Pnlip	Pancreatic triacylglycerol lipase	3,63****	2,66****	Secreted
Amy2	Pancreatic alpha-amylase Inactive	4,62****	1,67**	Secreted
Pnliprp1	pancreatic lipase-related protein 1	3,21****	1,84***	Secreted
Pnliprp2	Pancreatic lipase-related protein 2	2,92***	2,06****	Secreted
Alpi	Intestinal-type alkaline phosphatase 1	0,57*	1,02	Cell membrane
Cpa2	Carboxypeptidase A2	4,06****	2,58****	Secreted
Cpa1	Carboxypeptidase A1	4,02****	2,58****	Secreted
Cpb1	Carboxypeptidase B	4,26****	2,74****	Secreted
Cpa3	Mast cell carboxypeptidase A (Fragment)	2,50**	1,33	Secreted
Lct	Lactase-phlorizin hydrolase	0,26****	0,53***	Apical cell membrane
Anpep	Aminopeptidase N	0,32***	0,68*	Cell membrane
Si	Sucrase-isomaltase	0,43**	0,67*	Apical cell membrane
Try3	Cationic trypsin-3	6,76****	3,16****	Secreted
Dgat1	Diacylglycerol O-acyltransferase 1	0,32***	0,80	ER
Asah2	Neutral ceramidase	0,26****	0,52***	Cell membrane, Golgi apparatus, Mitochondrion, Secreted
Slc16a10	Monocarboxylate transporter 10	0,43	0,64	Basolateral cell membrane
Slc15a1	Solute carrier family 15 member 1	0,45*	0,91	Cell membrane
Slc7a8	Large neutral amino acids transporter small subunit 2	0,50	0,92	Basolateral cell membrane

Table 1 (continued)

Symbol	Description	Abundance ratio (<i>Atp7b</i> ^{-/-} / <i>Atp7b</i> WT)	Abundance ratio (<i>Atp7b</i> ^{-/-} diseased/ <i>Atp7b</i> WT)	Cellular localization
Slc6a19	Sodium-dependent neutral amino acid transporter B(0) AT1	0,47*	1,06	Apical cell membrane
Slc9a3	Sodium/hydrogen exchanger 3 Na(+)/H(+) exchange	0,31**	0,53**	Apical cell membrane
Slc9a3r1	regulatory cofactor NHE-RF1	0,30****	0,51****	Apical cell membrane
Slc39a4	Zinc transporter ZIP4	0,59	0,67	Cell membrane
Slc12a1	Solute carrier family 12 member 1	0,57	0,44***	Apical cell membrane
Slc2a5	Solute carrier family 2, facilitated glucose transporter member 5	0,41*	0,65	Apical cell membrane
Slc52a3	Solute carrier family 52, riboflavin transporter, member 3	0,36*	0,67	Cell membrane
Slc26a3	Chloride anion exchanger Na(+)/H(+) exchange	1,41	2,12****	Apical cell membrane
Slc9a3r2	regulatory cofactor NHE-RF2	2,06*	1,06	Apical cell membrane
Slc4a1	Band 3 anion transport protein	2,02*	1,16	Basolateral cell membrane
Chp2	Calcineurin B homologous protein 2	0,22****	0,47***	Cell membrane, Cytoplasm, Nucleus
Clic5	Chloride intracellular channel protein 5	0,48*	0,79	Apical cell membrane, Golgi apparatus, Cytoplasm, Cytoskeleton

*P < 0.05, **P < 0.01, ***P < 0.001, ****P < 0.0001.

significantly improved mitochondrial activity ($P = 0.0006$, for CCCP-treated cells) (Fig. 6B). Moreover, longer MB treatment of Caco-2 monolayers improved TEER values ($P = 0.0232$ at 21 days) (Fig. 6C), and cell-cell contact formation, observed by a more organized occludin pattern and increased presence of TJP-1 in MB-treated vs. untreated monolayers (Fig. 6D). Altogether, it appears that addition of the Cu chelator MB reverses the cellular aberrations of ATP7B-deficient intestinal epithelial cells, pleading in favour of the causal implication of Cu in this phenotype.

Methanobactin decreases copper content in the small intestine and ameliorates colon inflammation in Wilson disease rats.

To assess whether the gastrointestinal situation can also be ameliorated by Cu depletion in vivo, therapeutic chelation experiments were conducted in diseased WD rats (Supplementary Table 3). A pronounced Cu depletion in the small intestine of diseased WD rats was found upon MB treatment (i.p. injections of 110 mg/kg bw for eight days, sixteen total doses) in whole small intestine homogenates and cytosol ($P = 0.0791$) (Fig. 7A, B). In contrast, DPA (i.p. injections of 100 mg/kg, from three to eight days, six to sixteen total doses) had no effect on Cu levels in the whole small intestine homogenates (Fig. 7A), but significantly decreased Cu content in the cytosol ($P = 0.0041$). In support of these results, whole small tissue proteome analysis showed a decrease abundance of MT1/2, particularly in MB treated animals, in comparison to

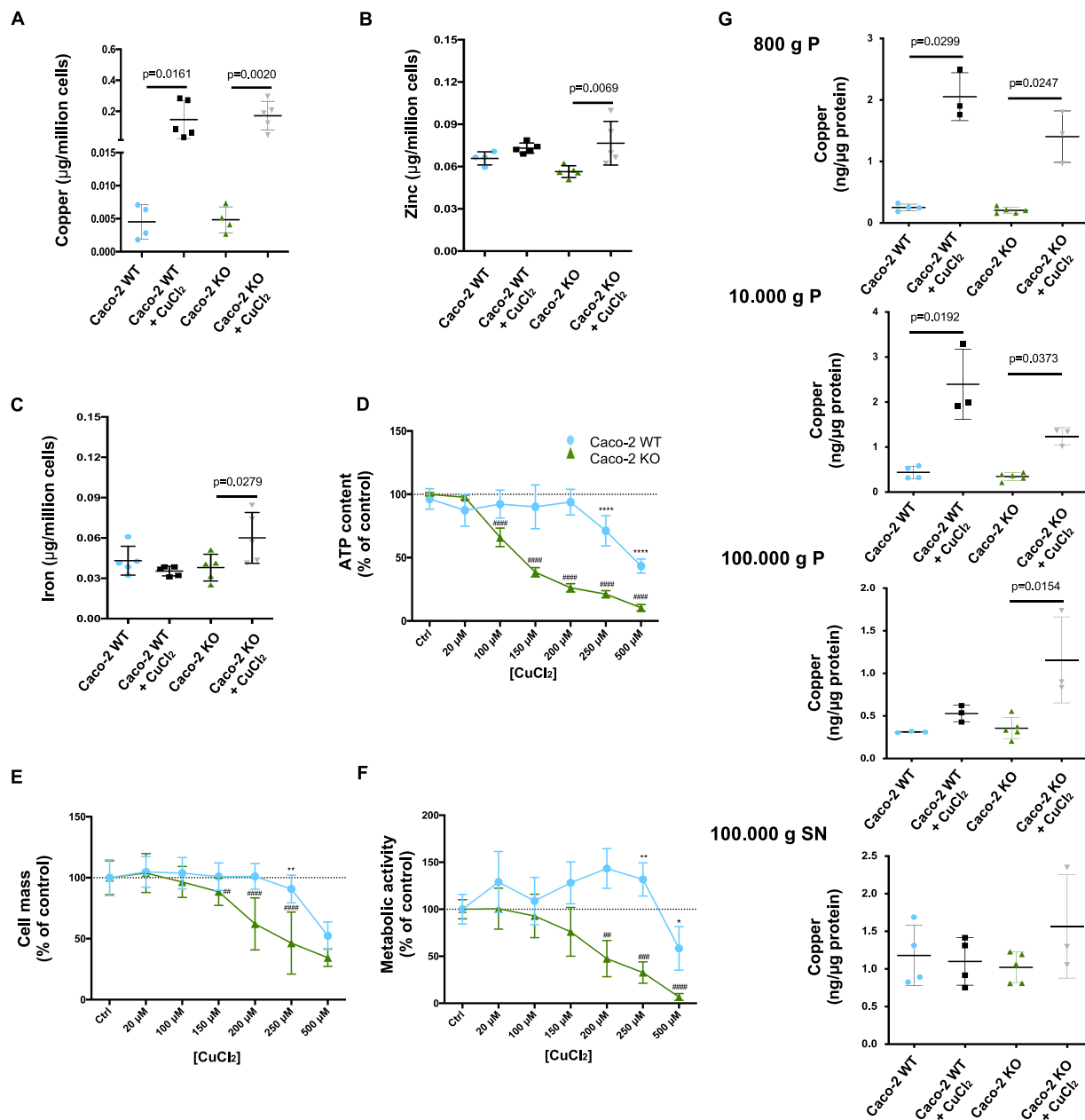


Fig. 5. Altered intracellular copper routing and increased copper sensitivity in Caco-2 *ATP7B* KO vs. WT cells. **(A)** A similar total cellular Cu content is measured in *ATP7B* KO vs. WT cells with/without Cu treatment. **(B)** Cellular zinc content is significantly increased in KO cells treated with Cu in comparison to controls **(C)** Cellular iron content is significantly increased in KO cells treated with Cu in comparison to control. **(D–F)** An increased Cu sensitivity in KO vs. WT cells is assessed in toxicity assays monitoring ATP cellular content, cellular mass, and metabolic activity. **(G)** Different copper contents upon Cu-challenge in subcellular fractions from KO vs. WT cells. Lower Cu-levels are found in the 800 g and 10.000 g fractions in KO vs. WT (containing cell debris/nuclei or mitochondria, respectively), but elevated ones in the 100.000 g pellet and supernatant fractions (vesicular and cytosolic fractions, respectively). Data are the mean \pm SD of $N = 4–5$ (A–C), $N = 3$ and $n = 3$ (D–F), One-way analysis of variance (Kruskal-Wallis), followed by Dunn's multiple comparisons test. *Significance to Caco-2 WT Control. #Significance to Caco-2 KO. * $P < 0.05$, ** $P < 0.01$, *** $P < 0.001$, **** $P < 0.0001$.

untreated diseased animals (Fig. 7C). In the light of the increased colon inflammation and structural alterations observed in humans, and both rodent models (Fig. 1), a closer examination at the colon of WD rats treated with MB was performed. An increased expression of the autophagy markers LC3b and p62 was observed in MB-treated animals, particularly after 1 and 1.5 days of treatment (Fig. 7E–F). For p62, the increased expression is less pronounced, however, the pathology pictures suggested a potential increase at the epithelium level, in comparison with the disease animals, where the expression was mostly present at the muscular mucosa (Fig. 7G). Mitochondria in the colon of diseased rats are more elongated and bigger in comparison to the mitochondria

upon MB-treatment, whose structure improves after 8 days of treatment, presenting a higher matrix density and more organized cristae (Fig. 7D).

Untreated WD rats developed clear signs of colonic inflammation, with a significant increase of the area occupied by immune cells (lymphocytes) in animals with no signs of liver disease ($P = 0.0035$) (Fig. 7H). Diseased animals that were treated with MB for 8-days were healthy at end of treatment (Supplementary Table 3), with no increase in colon inflammation when compared to the diseased control animals. In a direct comparison regarding disease state, meaning healthy, less inflammation is observed in the MB-treatment animals (Fig. 7H, I). Treatment with DPA was not as effective in improving both overall Cu

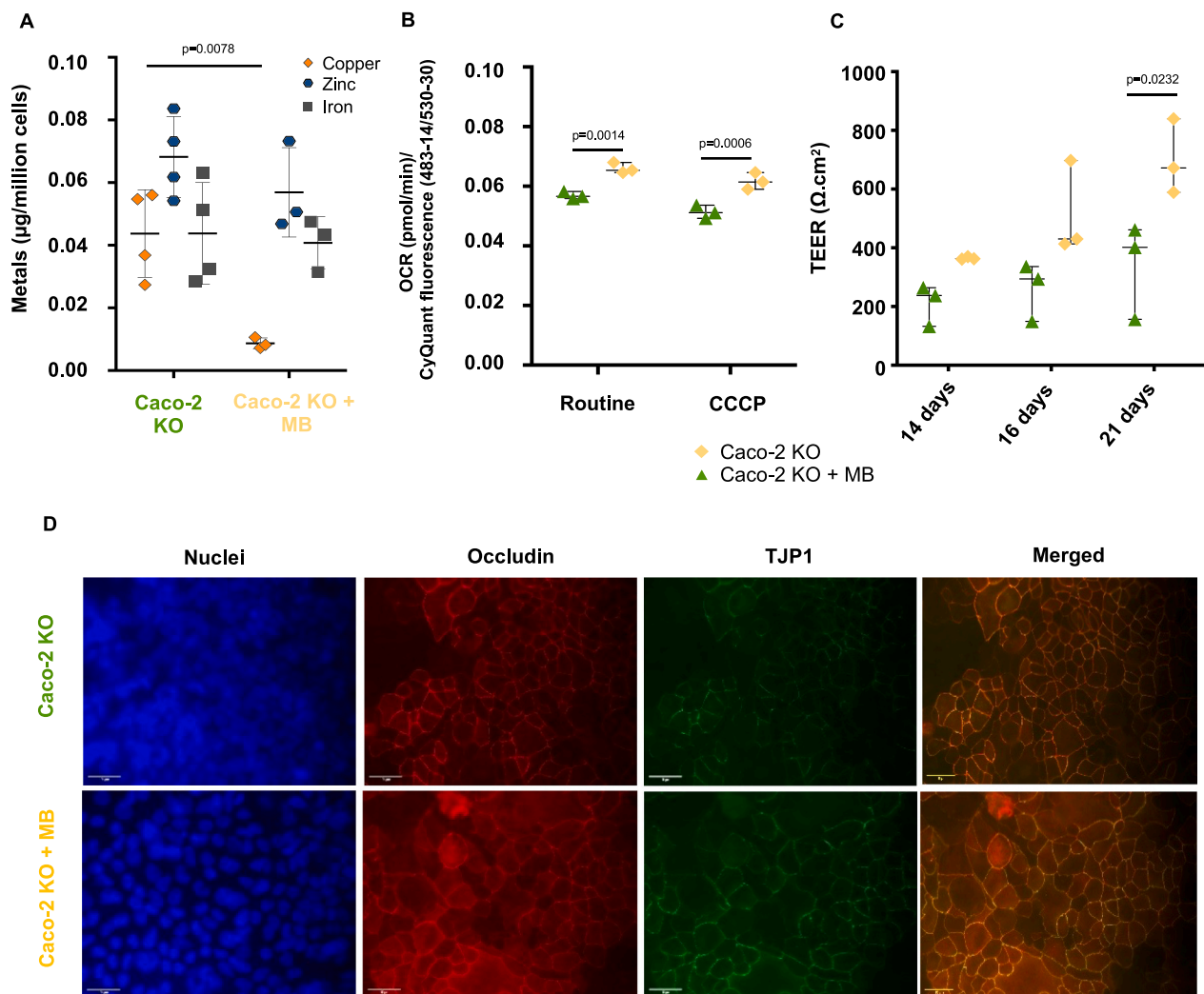


Fig. 6. Copper depletion restores mitochondrial function and cell-cell contacts in Caco-2 *ATP7B* KO cells. (A) Copper depletion is observed in KO monolayers upon treatment with Methanobactin (MB) (B) A treatment with MB for 24 h significantly improves mitochondrial oxygen consumption rate (OCR) in comparison to control. (C) MB increases the trans epithelial electrical resistance (TEER) in KO monolayers. (D) MB treatment of the KO monolayers increases the expression of the tight junction proteins occludin and TJP1 (scale bars: 10 µm). Data are the mean ± SD of N = 3–4 (A), N = 3, n = 3 (B), N = 3 (C). Two-way analysis of variance followed by Sidak's multiple comparisons test.

Table 2

Canonical pathway analysis of LPP *Atp7b*^{-/-} diseased rats upon treatment with MB or DPA.

Canonical pathways	-log(p-value)			z-score		
	<i>Atp7b</i> ^{-/-} D/ <i>Atp7b</i> ^{+/-}	<i>Atp7b</i> ^{-/-} D-MB/ <i>Atp7b</i> ^{-/-} D	<i>Atp7b</i> ^{-/-} D-DPA/ <i>Atp7b</i> ^{-/-} D	<i>Atp7b</i> ^{-/-} D/ <i>Atp7b</i> ^{+/-}	<i>Atp7b</i> ^{-/-} D-MB/ <i>Atp7b</i> ^{-/-} D	<i>Atp7b</i> ^{-/-} D-DPA/ DPA/ <i>Atp7b</i> ^{-/-} D
LXR/RXR Activation	9,06	6,12	1,64	-1941	2496	1342
DHCR24 Signaling Pathway	12,2	3,61	1,99	-2524	1291	0,816
Acute Phase Response Signaling	17,9	1,56	2,5	-1,5	0,333	0,447
Cholesterol biosynthesis	11,7	2,92	n.d.	3162	-2646	n.d.
Cholesterol Biosynthesis I	9,48	4,84	n.d.	2646	-2646	n.d.
Cholesterol Biosynthesis II (via 24,25-dihydrolanosterol)	9,48	4,84	n.d.	2646	-2646	n.d.
Cholesterol Biosynthesis III (via Desmosterol)	9,48	4,84	n.d.	2646	-2646	n.d.
Superpathway of Cholesterol Biosynthesis	10,9	2,18	n.d.	3162	-2646	n.d.
Activation of gene expression by SREBF (SREBP)	6,71	1,53	n.d.	2828	-2236	n.d.
IL-12 Signaling and Production in Macrophages	4,02	1,48	1,03	1941	-1265	-1633

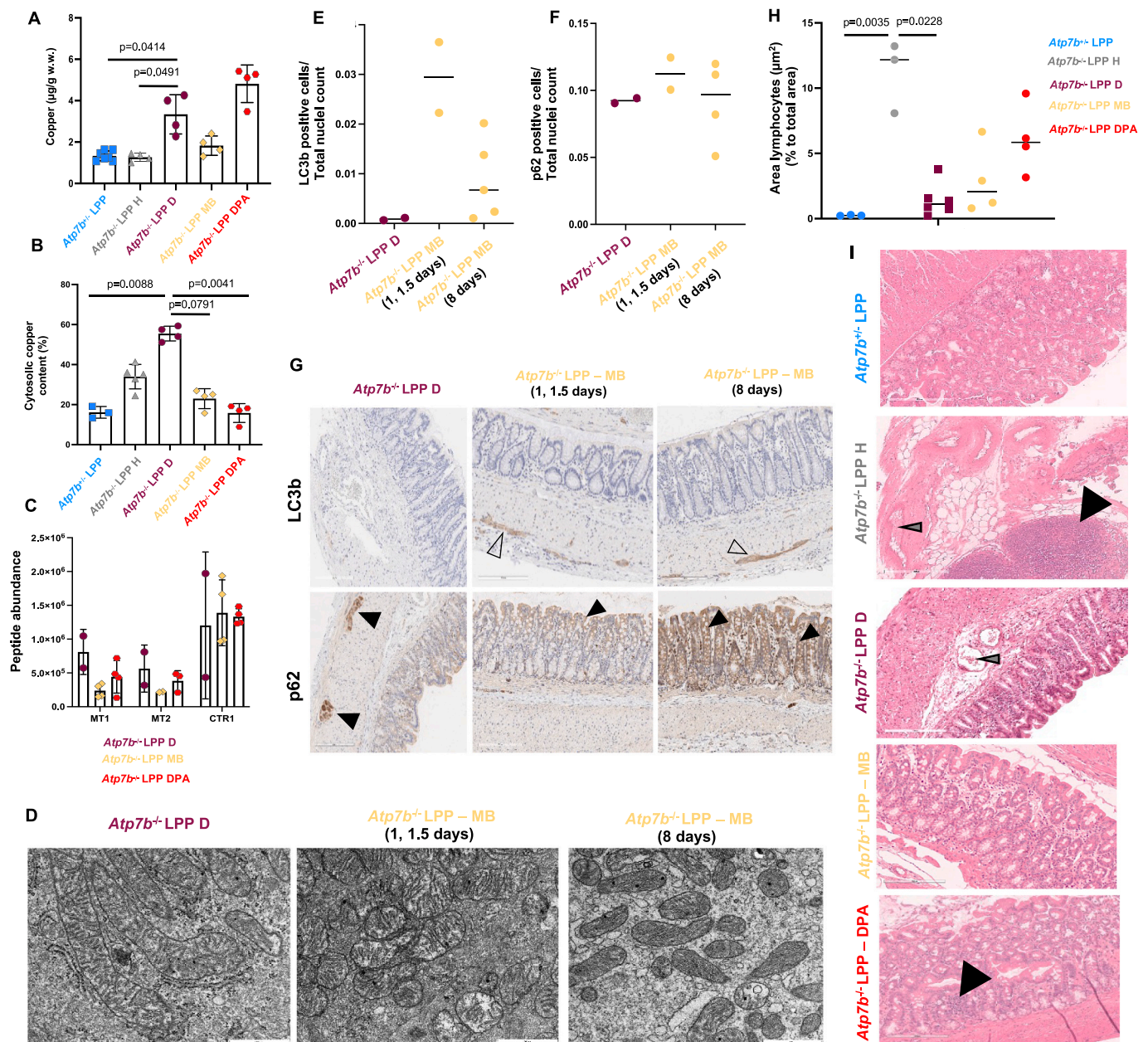


Fig. 7. Methanobactin (MB) promotes intestinal copper depletion in diseased WD rats and ameliorates colon inflammation. **(A)** Eight days of MB-, but not DPA-, treatment depletes total copper content in the small intestine of diseased WD rats. **(B)** As percentage to the total tissue copper content, both MB and DPA depleted cytosolic copper content. **(C)** Metallothionein 1 and 2 (MT1, 2) abundance was decreased in the small intestine upon MB treatment in comparison to diseased animals. **(D)** Mitochondria structure is altered upon MB-treatment, with increased matrix density and improved cristae organization (scale bar: 1000 nm). **(E-G)** One day MB treatment increased the expression of the autophagy marker LC3b, and promoted the epithelial expression of p62, versus the muscular mucosa localization observed in the colon of diseased animals (scale bar: 300 µm) **(E, F)** Eight days of MB-treatment was not as effective on the LC3b and p62 expression in the colon of WD rats. **(H)** Area occupied by lymphocytes in µm², as a % of the total tissue area in the colon of WD rats. The infiltration of lymphocytes is significantly increased in still healthy animals, with a higher decrease upon MB-treatment. **(I)** Mucosal infiltration (mainly lymphocytic, often in follicular arrangement, black arrow) in the colon of still healthy WD rats, and eosinophils (grey arrow) in both healthy and diseased WD rats, is mostly absent upon MB-, but not upon DPA-treatment. The latter still presenting with inflammation (black arrow) (scale bar: 300 µm). Data are the mean ± SD of $N = 2-7$. One-way analysis of variance (Kruskal-Wallis), followed by Dunn's multiple comparisons test.

content in the small intestine (Fig. 7A), or decreasing inflammation in the colon (Fig. 7H, I). Thus, successful Cu depletion with MB (but not DPA) blunts gut inflammation in this WD model. Moreover, the canonical pathway analysis of the small intestinal tissue proteome of disease animals clearly showed a significant inhibition of the LXR/RXR pathway ($-\log(p\text{-value}) > 1.3$, $z\text{-score} < -2$), with activation of the cholesterol biosynthesis and the IL-12 signaling and production of macrophages ($-\log(p\text{-value}) > 1.3$, $z\text{-score} > 2$). This scenario was significantly reversed upon MB treatment, but not by DPA (Table 2).

3. Discussion

Here, we reported intestinal inflammation affecting the small and large bowel of WD patients that underwent intestinal biopsies. In several WD-relevant models, namely ATP7B-deficient rats, mice and human colon epithelial cells we observed a similar pattern of malfunction (mitochondrial dysfunction with glycolytic shift and reduced intercellular junctions) that could be connected to subcellular Cu mislocalization in enterocytes. Both in cellular models and in WD rats, efficient Cu

chelation improved these defects.

Intestinal damage in Wilson disease – inflammation and decreased barrier integrity.

The presence of histologic alterations in small and large intestine in WD rats and *Atp7b*^{-/-} mice match the observations in WD patients, that reveals lymphocyte infiltration and distortion of crypts (Fig. 1). Intestinal homeostasis depends on the integrity of a tight enterocytic barrier, which is compromised in several inflammatory diseases that do not only affect the intestine, but also the liver [38,39]. Leaky gut syndrome can trigger liver inflammation via lipopolysaccharides and other microbe-associated molecular patterns that cross the gut barrier into the portal circulation [40]. In WD, indications of cellular barrier dysfunction were first suggested by Stuerenburg concerning the blood-brain barrier (BBB) [41], in agreement with later findings by Borchard and co-workers who reported significant Cu-induced damage to capillary endothelial cell monolayers [35]. Here we observed intestinal barrier dysfunction that manifests early, in apparently still healthy WD rats (Fig. 2G, H), and that is characterized by the depletion of key constitutive proteins such as claudins and adherent junctions [42], like E-cadherins (Fig. 2G). In comparison to their WT counterparts, *Atp7b*^{-/-} mice manifested similar structural alterations in the small intestine (Fig. 2I). To further study this phenomenon at the cellular level, Caco-2 *ATP7B* KO cells were used as a surrogate of human WD enterocytes (Supplementary Fig. 2A) [33]. These cells differentiate to enterocyte-like cells in a Transwell system [43] (Supplementary Fig. 3A) and have the capacity to regulate Cu uptake [44]. Moreover, Cu toxicity has been reported to affect Caco-2 WT cells, leading to a decrease in TEER [45] and TJ dysfunction [46]. Of note, barrier formation was compromised in Caco-2 *ATP7B* KO cells, with lower TEER (Fig. 4A), decreased protein abundance of occludin and claudin 4 (Fig. 4B), widening of the cell-cell adhesion spaces (Fig. 4C) and decreased/disorganized expression of major TJ proteins, as compared to WT cells (Fig. 4D). Together with the relevant and unexpected finding of a potential leaky gut affecting WD rats, marked alterations in lipid metabolism (Supplementary Tables 1 and 2), mitochondrial dysfunction (Fig. 2F, H, Fig. 3, Supplementary Table 2) and a metabolic shift to glycolysis (Table 1, Supplementary Table 2, Fig. 3F, Supplementary Fig. 2C) were observed in both WD rats and Caco-2 KO cells. These pathological aspects manifested already early in the disease, before hepatitis onset, and therefore might be potentially relevant for disease pathogenesis. In agreement with this consideration, it is most compelling that mice bearing a whole-body *Atp7b*^{-/-} knockout (that also affects the gut), develop a more pronounced liver damage and earlier progression to fatal disease than mice bearing a hepatocyte-specific *Atp7b*^{-/-} knockout [47].

Mitochondrial dysfunction affecting enterocytes in Wilson disease.

Structural and functional alterations affecting hepatocyte mitochondria are a hallmark in WD, as the main hub for Cu storage and utilization in the hepatocytes [3–5]. In this study, mitochondrial structure alterations were also prominently visible in the small intestine of still healthy WD rats and *Atp7b*^{-/-} mice (Fig. 2H, I), agreeing with previous findings in *Atp7b*^{-/-} mice [16]. In addition, proteome analysis from the small intestine of WD rats showed significant changes in important proteins linked to mitochondrial organization/renewal and bioenergetic function (Fig. 2F, Table 1). Importantly, however, these WD intestinal mitochondrial structure impairments differ substantially from WD liver mitochondria (Supplementary Fig. 1). While WD liver mitochondrial structures are progressively directly disturbed by an increasing Cu burden [30–32], this is not the case for WD intestinal mitochondria. Neither have we observed an increased mitochondrial Cu content in Caco-2 *ATP7B* KO cells, nor did an additional Cu-challenge raise the mitochondrial Cu above the levels observed in WT control mitochondria (Fig. 5G). Thus, excessive local Cu levels are unlikely to directly damage enterocyte mitochondria in WD, contrasting with its well-documented toxic effects on hepatocyte mitochondria [4,32]. Nonetheless, the Caco-2 *ATP7B* KO cells are more sensitive to increasing Cu concentrations (Fig. 5D–F), with Cu-depletion by MB being able to

improve mitochondria function and barrier integrity, even without previous Cu burden (Fig. 6). These results indicate a negative effect of Cu on intestinal mitochondria, most plausibly as a secondary event related to its increase in nonmitochondrial subcellular compartments such as the cytosol and a yet-to-be-defined vesicular fraction (Fig. 5G). Dysfunctional mitochondria are typically degraded by autophagy (that then is referred to as ‘mitophagy’) that relies on intact lysosomes. Indeed, our proteome comparisons of *ATP7B* KO and WT cells not only revealed KO-associated deficits in mitochondrial but also in lysosomal biogenesis and function (Supplementary Fig. 2B1). Thus, both mitochondrial biogenesis and turnover may be affected by *ATP7B* deficiency, and consequent MB-repressible alterations in Cu handling by cells. In the WD rats, Cu elevation in the small intestine was decreased by MB-treatment, with a concomitant decrease in the cytosolic Cu-binding proteins MT1 and 2 (Fig. 7A–C). In parallel, elevation in the relative amount of LC3b and p62 in the colon (Fig. 7D–F), along with a decrease in inflammation (Fig. 7H, I, Table 2), and mitochondria improved structure (Fig. 7D), indicates a potential induction of autophagy by MB treatment (Fig. 7D–G).

The regulation of lipid metabolism is also impaired in WD rats, with a significant activation of cholesterol biosynthesis pathways, along with a significant inhibition of cholesterol traffic and efflux (Table 2). A potential impairment of chylomicrons assembly and export at the level of the enterocytes was previously described in *Atp7b*^{-/-} mice [16], which also present with mitochondria structural alterations and decreased barrier integrity (Fig. 2I). Furthermore, intestinal epithelial cells of KO mice with reduced formation of OXPHOS supercomplexes, or specific ablation of OXPHOS subunits presented with large lipid droplets in the small intestine tissue, but decreased content of TG in the liver, demonstrating a direct connection between mitochondria dysfunction and lipid accumulation with subsequent impaired lipid transport [48]. In the present study, treatment with MB ameliorated lipid dysfunction in the small intestine of WD rats (Table 2), further supporting the possible induction of mitochondria turnover. Clearly, further studies must unravel the Cu-dependent signaling and mechanistic events underlying these mitochondrial and cellular alterations. Nevertheless, it appears that the compromised mitochondrial bioenergetic capacity, plausibly due to impaired turnover, is accompanied to less tight intestinal cell-cell contact, lipid metabolism dysregulation and inflammation in the intestine of WD rats. A recent paper by Solier and co-workers demonstrated that subformin-mediated Cu chelation in monocyte-derived macrophages had anti-inflammatory effects both in vitro and in vivo, including in a model of acute intestinal perforation [49]. These findings suggest a proinflammatory role for Cu, that is substantiated by our findings as well.

This new evidence is of potential importance for WD patients, since currently it is hard to predict disease progression. A diagnosis confirming intestinal leakiness and inflammation at an early disease stage could plausibly help in disease management with therapies that aim to restore gut health and thereby improve the quality of life of WD patients. Furthermore, the presence of an intestinal phenotype could further aid physicians to decide on a better course of treatment, or even use it as a diagnosis tool since it precedes clinical signs of liver damage. Interestingly, the same features are observed in patients that suffer from intestinal bowel diseases (IBD), including hepatobiliary disorders [50,51] and, in specific cases, elevated copper concentrations in liver [52], serum [53,54] and urine [55]. Moreover, it was recently suggested that Cu-induced regulated cell death dubbed cuproptosis plays an important role in the pathogenesis of IBD [56]. Even though the incidence of IBD [57,58] largely outnumbers that of WD [59], this phenotypic correlation appears intriguing, warranting further mechanistic exploration. In this context, it might be interesting to explore the anti-inflammatory effects of copper chelators (that have been reported for triethylene tetraamine [60] and subformin [49]) on prevalent intestinal pathologies such as colitis ulcerosa and Crohn’s disease.

4. Conclusion

In conclusion, we report intestinal inflammation in WD patients and preclinical WD models, along with metabolic alterations, mitochondrial dysfunction, and small intestine barrier leakiness. As GI tract issues are not typically analysed in WD patients, the number of human WD samples in this study was very limited, thus needing future validation. Especially the barrier leakiness may account for colonic inflammation as well as for the aggravation of hepatic alterations. Our results further show that the Cu-chelator methanobactin (MB) can restore some of the observed features in both in vitro and in vivo models. Therefore, the mechanisms behind this MB action against the Cu imbalance scenario in the GI tract require future elucidation. To this point, in both liver and intestine, the fast amelioration observed in the animals upon MB treatment is likely related to cellular renewal processes possibly involving autophagy. To this, further studies are warranted, such as functional in vivo assays to better understand mitochondria/lysosomal function, and a more detailed evaluation of the GI mucosa in both animal models and WD patients with regards to inflammation and autophagy.

Supplementary data to this article can be found online at <https://doi.org/10.1016/j.metabol.2024.155973>.

Significance of the study:

What is already known on this topic?

- Fourty % of Wilson disease (WD) patients exhibit gastrointestinal symptoms that are often encountered before diagnosis or as a consequence of zinc salt therapy.
- Therapeutical options for WD are limited, and the incidence of adverse effects including neurological problems is high. Therefore, new treatments are urgently needed.
- A poor genotype-phenotype relation suggests a major impact of environmental factors beyond copper exposure for disease progression.

What this study adds?

- Intestinal inflammation is present in WD patients, as well as in WD animal models.
- Mice and rats lacking ATP7B manifest mitochondrial structural alterations in enterocytes and compromised gut barrier integrity before hepatic destruction.
- Human ATP7B KO colon cancer cells also exhibit mitochondrial dysfunction and the incapacity to form tight monolayers.
- Treatment with the copper chelator methanobactin ameliorates the intestinal phenotype of ATP7B-deficient rats and the alterations of ATP7B-null human colon cancer cells.

How this study might affect research, practice or policy?

- In clinical practice, evidence of an intestinal phenotype may accelerate and ameliorate patient diagnosis, allowing the implementation of personalized therapies.
- Our study should stimulate the exploration of potential new WD-relevant biomarkers linked to changes in gut barrier tightness and inflammation.
- The results present in this study adds to the comprehension of the extrahepatic consequences of ATP7B deficiency.

Author contributions

A.F., H.P., B.A., J.K., T.R., J.S. and Q.R. designed and/or performed experiments. C.E. performed EM analysis. F.N., K.S. O-S, J.CK. and S.S. performed pathology analysis. C.vT. and S.M.H. performed proteome analysis. B.M. and Q.R. performed metal analyses. J.D.S., A.M.D. and A.

A.D. performed MB isolation and purification. A.Z. and H.H.S. established knock out cell lines. A.F., H.P., J.B., A.M.A. and S.L. performed data analysis. H.Z., A.M.A, J.R.S, S.L. and P.S. obtained funding and supervised this study. A.F., H.P., P.S., S.L., R.P., G.K. and H.Z. wrote the manuscript. All authors reviewed and provided feedback towards the final manuscript. H.Z. directed this study.

Funding

The authors' work was supported by the FOIE GRAS and mtFOIE GRAS projects. These projects received funding from the European Union's Horizon 2020, Research and Innovation programme under the Marie Skłodowska-Curie Grant Agreement No. 722619 (FOIE GRAS) and Grant Agreement No. 734719 (mtFOIE GRAS). This research work was also developed under the Portuguese national funds via FCT—Fundação para a Ciência e a Tecnologia with the FCT grant SFRH/BD/05623/2020 and the National Institute of Health DK071865-14A1. Further funding for parts of this work came from the Bundesministerium für Bildung und Forschung (BMBF) (Project "WilsonMed – Multimolecular Targeting of Copper Overload in Wilson's Disease", grant 01GM2001B, European Joint Program on Rare Diseases) and from the Deutsche Forschungsgemeinschaft (DFG) grant ZI 1386/2–1. GK has been holding research contracts with Daiichi Sankyo, Eleor, Kaleido, Lytix Pharma, PharmaMar, Osasuna Therapeutics, Samsara Therapeutics, Sanofi, Tollys, and Vascage. GK is on the Board of Directors of the Bristol Myers Squibb Foundation France. GK is a scientific co-founder of everImmune, Osasuna Therapeutics, Samsara Therapeutics and Therafast Bio. GK is in the scientific advisory boards of Hevolution, Institut Servier, Longevity Vision Funds and Rejuveron Life Sciences. GK is the inventor of patents covering therapeutic targeting of aging, cancer, cystic fibrosis and metabolic disorders. GK's wife, Laurence Zitvogel, has held research contracts with Glaxo Smyth Kline, Incyte, Lytix, Kaleido, Innovate Pharma, Daiichi Sankyo, Pilege, Merus, Transgene, 9 m, Tusk and Roche, was on the Board of Directors of Transgene, is a cofounder of everImmune, and holds patents covering the treatment of cancer and the therapeutic manipulation of the microbiota. GK's brother, Romano Kroemer, was an employee of Sanofi and now consults for Boehringer-Ingelheim. The funders had no role in the design of the study; in the writing of the manuscript, or in the decision to publish the results.

CRediT authorship contribution statement

Adriana Fontes: Writing – review & editing, Writing – original draft, Methodology, Formal analysis, Data curation, Conceptualization. **Hannah Pierson:** Writing – original draft, Visualization, Methodology, Formal analysis, Data curation, Conceptualization. **Joanna B. Bierła:** Methodology, Investigation, Formal analysis, Data curation, Conceptualization. **Carola Eberhagen:** Software, Formal analysis. **Jennifer Kinschel:** Formal analysis, Data curation. **Banu Akdogan:** Resources, Methodology, Formal analysis, Data curation. **Tamara Rieder:** Methodology, Investigation. **Judith Sailer:** Methodology, Formal analysis. **Quirin Reinold:** Methodology, Formal analysis, Data curation. **Joanna Cielecka-Kuszyk:** Methodology, Formal analysis. **Sylwia Szymańska:** Methodology, Formal analysis. **Frauke Neff:** Validation. **Katja Steiger:** Validation, Supervision. **Olga Seelbach:** Methodology, Formal analysis. **Andree Zibert:** Resources, Methodology. **Hartmut H. Schmidt:** Supervision, Resources. **Stefanie M. Hauck:** Supervision. **Christine von Toerne:** Writing – review & editing, Methodology, Formal analysis, Data curation. **Bernhard Michalke:** Methodology, Formal analysis, Data curation. **Jeremy D. Semrau:** Resources. **Ana M. DiSpirito:** Resources. **João Ramalho-Santos:** Writing – review & editing, Supervision. **Guido Kroemer:** Writing – review & editing. **Roman Polishchuk:** Writing – review & editing, Supervision, Resources. **Anabela Marisa Azul:** Writing – review & editing, Supervision, Funding acquisition. **Alan DiSpirito:** Resources. **Piotr Socha:** Writing – review & editing, Supervision, Funding acquisition. **Svetlana Lutsenko:** Writing –

original draft, Supervision, Formal analysis, Conceptualization. **Hans Zischka**: Writing – review & editing, Supervision, Funding acquisition, Conceptualization.

Declaration of competing interest

HZ is scientific consultant for ArborMed Co. Ltd. GK is supported by the Ligue contre le Cancer (équipe labellisée); Agence Nationale de la Recherche (ANR) – Projets blancs; AMMICA US23/CNRS UMS3655; Association pour la recherche sur le cancer (ARC); Cancéropôle Ile-de-France; Fondation pour la Recherche Médicale (FRM); a donation by Elior; Equipex Onco-Pheno-Screen; European Joint Programme on Rare Diseases (EJPRD); European Research Council Advanced Investigator Award (ERC-2021-ADG, ICD-Cancer, Grant No. 101052444), European Union Horizon 2020 Projects Oncobiome, Prevalung (grant No. 101095604) and Crimson; Institut National du Cancer (INCA); Institut Universitaire de France; LabEx Immuno-Oncology ANR-18-IDEX-0001; a Cancer Research ASPIRE Award from the Mark Foundation; the RHUs Immunolife and LUCA-pi; Seerave Foundation; SIRIC Stratified Oncology Cell DNA Repair and Tumor Immune Elimination (SOCRATE); and SIRIC Cancer Research and Personalized Medicine (CARPEM). This study contributes to the IdEx Université de Paris ANR-18-IDEX-0001. Views and opinions expressed are those of the author(s) only and do not necessarily reflect those of the European Union, the European Research Council or any other granting authority. Neither the European Union nor any other granting authority can be held responsible for them.

Acknowledgments

The authors would especially like to thank the Morbus Wilson e.V. for the generous financial support that enabled the acquisition of a CellScope device.

References

- Członkowska A, Litwin T, Dusek P, et al. Wilson disease. *Nat Rev Dis Primers* Sep 6 2018;4(1):21. <https://doi.org/10.1038/s41572-018-0018-3>.
- Gitlin JD. Wilson disease. *Gastroenterology* Dec 2003;125(6):1868–77. <https://doi.org/10.1053/j.gastro.2003.05.010>.
- Sternlieb I. Mitochondrial and fatty changes in hepatocytes of patients with Wilson's disease. *Gastroenterology* Sep 1968;55(3):354–67.
- Zischka H, Lichtmanegger J. Pathological mitochondrial copper overload in livers of Wilson's disease patients and related animal models. *Ann N Y Acad Sci* May 2014;1315:6–15. <https://doi.org/10.1111/nyas.12347>.
- Zischka H, Einer C. Mitochondrial copper homeostasis and its derailment in Wilson disease. *Int J Biochem Cell Biol* Sep 2018;102:71–5. <https://doi.org/10.1016/j.biocel.2018.07.001>.
- Polishchuk EV, Concilli M, Iacobacci S, et al. Wilson disease protein ATP7B utilizes lysosomal exocytosis to maintain copper homeostasis. *Dev Cell* Jun 23 2014;29(6):686–700. <https://doi.org/10.1016/j.devcel.2014.04.033>.
- Polishchuk EV, Merolla A, Lichtmanegger J, et al. Activation of Autophagy, Observed in Liver Tissues From Patients With Wilson Disease and From ATP7B-Deficient Animals, Protects Hepatocytes From Copper-Induced Apoptosis. *Gastroenterology* Mar 2019;156(4):1173–89. e5. <https://doi.org/10.1053/j.gastro.2018.11.032>.
- Klein D, Arora U, Lichtmanegger J, Finckh M, Heinzmann U, Summer KH. Tetrathiomolybdate in the treatment of acute hepatitis in an animal model for Wilson disease. *J Hepatol* Mar 2004;40(3):409–16. <https://doi.org/10.1016/j.jhep.2003.11.034>.
- Stremmel W, Weiskirchen R. Therapeutic strategies in Wilson disease: pathophysiology and mode of action. *Ann Transl Med* Apr 2021;9(8):732. <https://doi.org/10.21037/atm-20-3090>.
- European Association for Study of L. EASL clinical practice guidelines: Wilson's disease. *J Hepatol* Mar 2012;56(3):671–85. <https://doi.org/10.1016/j.jhep.2011.11.007>.
- Kenney SM, Cox DW. Sequence variation database for the Wilson disease copper transporter, ATP7B. *Hum Mutat* Dec 2007;28(12):1171–7. <https://doi.org/10.1002/humu.20586>.
- Kieffer DA, Medici V. Wilson disease: at the crossroads between genetics and epigenetics—a review of the evidence. *Liver Res.* 2017/09/01;1(2):121–30. <https://doi.org/10.1016/j.livres.2017.08.003>.
- Einer C, Leitzinger C, Lichtmanegger J, et al. A high-calorie diet aggravates mitochondrial dysfunction and triggers severe liver damage in Wilson disease rats. *Cell Mol Gastroenterol Hepatol* 2019;7(3):571–96. <https://doi.org/10.1016/j.jcmgh.2018.12.005>.
- Linder MC. Copper homeostasis in mammals, with emphasis on secretion and excretion. A review. *Int J Mol Sci* Jul 13 2020;21(14). <https://doi.org/10.3390/ijms21144932>.
- Weiss KH, Wurz J, Gotthardt D, Merle U, Stremmel W, Füllekrug J. Localization of the Wilson disease protein in murine intestine. *J Anat* 2008. <https://doi.org/10.1111/j.1469-7580.2008.00954.x>.
- Pierson H, Muchenditsi A, Kim BE, et al. The function of ATPase copper transporter ATP7B in intestine. *Gastroenterology* Jan 2018;154(1):168–80. e5. <https://doi.org/10.1053/j.gastro.2017.09.019>.
- Guttman S, Nadzemova O, Grünwald I, et al. ATP7B knockout disturbs copper and lipid metabolism in Caco-2 cells. *PLoS One* 2020;15(3):e0230025. <https://doi.org/10.1371/journal.pone.0230025>.
- Jang HJ, Jang JY, Kim K-M. Appendiceal orifice inflammation in an 8-year-old girl with ulcerative colitis complicating Wilson's disease. *Gut Liver* 2010. <https://doi.org/10.5009/gnl.2010.4.1.126>.
- Nery FG, Marques I, Magalhães M, Miranda HP. Wilson's disease and ulcerative colitis in the same patient: just a coincidence? A case report and literature review. *Gastroenterol Res* Dec 2010;3(6):287–9. <https://doi.org/10.4021/gr271w>.
- Toritsu T, Esaki M, Matsumoto T, et al. A rare case of ulcerative colitis complicating Wilson's disease. *J Clin Gastroenterol* 2002. <https://doi.org/10.1097/00004836-200207000-00010>.
- Cai X, Deng L, Ma X, et al. Altered diversity and composition of gut microbiota in Wilson's disease. *Sci Rep* Dec 11 2020;10(1):21825. <https://doi.org/10.1038/s41598-020-78988-7>.
- Geng H, Shu S, Dong J, et al. Association study of gut flora in Wilson's disease through high-throughput sequencing. *Medicine (Baltimore)* Aug 2018;97(31):e11743. <https://doi.org/10.1097/md.00000000000011743>.
- Sarode GV, Mazi TA, Neier K, et al. The role of intestine in metabolic dysregulation in murine Wilson disease. *bioRxiv* Jan 14 2023. <https://doi.org/10.1101/2023.01.13.524009>.
- Camarata MA, Ala A, Schilsky ML. Zinc maintenance therapy for Wilson disease: a comparison between zinc acetate and alternative zinc preparations. *Hepatol Commun* Aug 2019;3(8):1151–8. <https://doi.org/10.1002/hep4.1384>.
- Mohr I, Weiss KH. Current anti-copper therapies in management of Wilson disease. *Ann Transl Med* Apr 2019;7(Suppl. 2):S69. <https://doi.org/10.21037/atm.2019.02.48>.
- Wiernicka A, Jańczyk W, Dądalski M, Avsar Y, Schmidt H, Socha P. Gastrointestinal side effects in children with Wilson's disease treated with zinc sulphate. *World J Gastroenterol* Jul 21 2013;19(27):4356–62. <https://doi.org/10.3748/wjg.v19.i27.4356>.
- EASL Clinical Practice Guidelines. Wilson's disease. *J Hepatol* Mar 2012;56(3):671–85. <https://doi.org/10.1016/j.jhep.2011.11.007>.
- Roberts EA. Update on the diagnosis and Management of Wilson Disease. *Curr Gastroenterol Rep* Nov 5 2018;20(12):56. <https://doi.org/10.1007/s11894-018-0660-7>.
- Sturniolo GC, Mestriner C, Irato P, Albergoni V, Longo G, D'Inca R. Zinc therapy increases duodenal concentrations of metallothionein and iron in Wilson's disease patients. *Am J Gastroenterol* Feb 1999;94(2):334–8. <https://doi.org/10.1111/j.1572-0241.1999.851.w.x>.
- Einer C, Munk DE, Park E, et al. ARBM101 (Methanobactin SB2) Drains Excess Liver Copper via Biliary Excretion in Wilson's Disease Rats. *Gastroenterology* Mar 24 2023. <https://doi.org/10.1053/j.gastro.2023.03.216>.
- Lichtmanegger J, Leitzinger C, Wimmer R, et al. Methanobactin reverses acute liver failure in a rat model of Wilson disease. *J Clin Invest* 07/01/2016;126(7):2721–35. <https://doi.org/10.1172/JCI85226>.
- Zischka H, Lichtmanegger J, Schmitt S, et al. Liver mitochondrial membrane crosslinking and destruction in a rat model of Wilson disease. *J Clin Invest* Apr 2011;121(4):1508–18. <https://doi.org/10.1172/jci45401>.
- Guttman S, Nadzemova O, Grünwald I, et al. ATP7B knockout disturbs copper and lipid metabolism in Caco-2 cells. *PLoS One* 2020. <https://doi.org/10.1371/journal.pone.0230025>.
- Berger E, Rath E, Yuan D, et al. Mitochondrial function controls intestinal epithelial stemness and proliferation. *Nat Comm* 2016/10/27;7(1):13171. <https://doi.org/10.1038/ncomms13171>.
- Borchard S, Raschke S, Zak KM. Bis-choline tetrathiomolybdate prevents copper-induced blood-brain barrier damage. *Life Sci Alliance* Mar 2022;5:3. <https://doi.org/10.26508/lsa.202101164>.
- JanssenDuijghuijsen LM, Grefte S, de Boer VCJ, et al. Mitochondrial ATP depletion disrupts Caco-2 monolayer integrity and internalizes Claudin 7. *Front Physiol* 2017;8:794. <https://doi.org/10.3389/fphys.2017.00794>.
- Linz G, Djeljadini S, Steinbeck L, Köse G, Kiessling F, Wessling M. Cell barrier characterization in transwell inserts by electrical impedance spectroscopy. *Biosens Bioelectron* 2020/10/01;165:112345. <https://doi.org/10.1016/j.bios.2020.112345>.
- Mandato C, Delli Bovi AP, Vajro P. The gut-liver axis as a target of liver disease management. *Hepatobiliary Surg Nutr* Jan 2021;10(1):100–2. <https://doi.org/10.21037/hbsn.2020.03.27>.
- Vancamelbeke M, Vermeire S. The intestinal barrier: a fundamental role in health and disease. *Expert Rev Gastroenterol Hepatol* Sep 2017;11(9):821–34. <https://doi.org/10.1080/17474124.2017.1343143>.
- Di Ciaula A, Baj J. Liver Steatosis, Gut-Liver Axis, Microbiome and Environmental Factors. A Never-Ending Bidirectional Cross-Talk. *J Clin Med* Aug 14 2020;9(8). <https://doi.org/10.3390/jcm9082648>.
- Stuerenburg HJ. CSF copper concentrations, blood-brain barrier function, and coeruleoplasm synthesis during the treatment of Wilson's disease. *J Neural*

- Transm (Vienna, Austria: 1996) 2000;107(3):321–9. <https://doi.org/10.1007/s007020050026>.
- [42] Garcia MA, Nelson WJ, Chavez N. Cell-cell junctions organize structural and signaling networks. *Cold Spring Harb Perspect Biol* Apr 2 2018;10(4). <https://doi.org/10.1101/cshperspect.a029181>.
- [43] Natoli M, Leoni BD, D'Agnano I, Zucco F, Felsani A. Good Caco-2 cell culture practices. *Toxicol In Vitro* Dec 2012;26(8):1243–6. <https://doi.org/10.1016/j.tiv.2012.03.009>.
- [44] Zerounian NR, Redekosky C, Malpe R, Linder MC. Regulation of copper absorption by copper availability in the Caco-2 cell intestinal model. *Am J Physiol Gastrointest Liver Physiol* May 2003;284(5):G739–47. <https://doi.org/10.1152/ajpgi.00415.2002>.
- [45] Ferruzza S, Scacchi M, Scarino ML, Sambuy Y. Iron and copper alter tight junction permeability in human intestinal Caco-2 cells by distinct mechanisms. *Toxicol In Vitro* Aug 2002;16(4):399–404. [https://doi.org/10.1016/s0887-2333\(02\)00020-6](https://doi.org/10.1016/s0887-2333(02)00020-6).
- [46] Ude VC, Brown DM, Viale L, Kanase N, Stone V, Johnston HJ. Impact of copper oxide nanomaterials on differentiated and undifferentiated Caco-2 intestinal epithelial cells; assessment of cytotoxicity, barrier integrity, cytokine production and nanomaterial penetration. *Part Fibre Toxicol* 2017;08/23;14(1):31. <https://doi.org/10.1186/s12989-017-0211-7>.
- [47] Muchenditsi A. Systemic deletion of Atp7b modifies the Hepatocytes' response to copper overload in the mouse models of Wilson disease. *FASEB J* 2021;35(S1). <https://doi.org/10.1096/fasebj.2021.35.S1.02946>.
- [48] Moschandrea C, Kondylis V, Evangelakos I, et al. Mitochondrial dysfunction abrogates dietary lipid processing in enterocytes. *Nature* 12/20 2023;625:1–8. <https://doi.org/10.1038/s41586-023-06857-0>.
- [49] Solier S, Müller S, Cañeque T, et al. A druggable copper-signalling pathway that drives inflammation. *Nature* May 2023;617(7960):386–94. <https://doi.org/10.1038/s41586-023-06017-4>.
- [50] Danese S, Semeraro S, Papa A, et al. Extraintestinal manifestations in inflammatory bowel disease. *World J Gastroenterol* Dec 14 2005;11(46):7227–36. <https://doi.org/10.3748/wjg.v11.i46.7227>.
- [51] Veltkamp C, Lan S, Korompoki E, Weiss K-H, Schmidt H, Seitz HK. Hepatic steatosis and fibrosis in chronic inflammatory bowel disease. *J Clin Med* 2022;11(9):2623.
- [52] Ritland S, Elgjo K, Johansen O, Steinnes E. Liver copper content in patients with inflammatory bowel disease and associated liver disorders. *Scand J Gastroenterol* 1979/09/01;14(6):711–5. <https://doi.org/10.3109/00365527909181942>.
- [53] Ringstad J, Kildebo S, Thomassen Y. Serum selenium, copper, and zinc concentrations in Crohn's disease and ulcerative colitis. *Scand J Gastroenterol Jul* 1993;28(7):605–8. <https://doi.org/10.3109/00365529309096096>.
- [54] Dalekos GN, Ringstad J, Savaidis I, Seferiadis KI, Tsianos EV. Zinc, copper and immunological markers in the circulation of well nourished patients with ulcerative colitis. *Eur J Gastroenterol Hepatol* 1998;10(4).
- [55] Ince AT, Kayadibi H, Soylu A, et al. Serum copper, Ceruloplasmin and 24-h urine copper evaluations in celiac patients. *Dig Dis Sci* 2008/06/01;53(6):1564–72. <https://doi.org/10.1007/s10620-007-0043-7>.
- [56] Chen Y, Li X, Sun R, et al. A broad cuproptosis landscape in inflammatory bowel disease. Original research. *Front Immunol* 2022-November-03;13. <https://doi.org/10.3389/fimmu.2022.1031539>.
- [57] Aniwan S, Santiago P, Loftus EV, Park SH. The epidemiology of inflammatory bowel disease in Asia and Asian immigrants to Western countries. *United Eur Gastroenterol J* 2022. <https://doi.org/10.1002/ueg2.12350>.
- [58] Zhao M, Gönczi L, Lakatos L, Burisch J. The burden of inflammatory bowel disease in Europe in 2020. *J Crohns Colitis* 2021. <https://doi.org/10.1093/ecco-jcc/jjab029>.
- [59] Liu J, Luan J, Zhou X, Cui Y, Han J. Epidemiology, diagnosis, and treatment of Wilson's disease. *Intractable Rare Dis Res* Nov 2017;6(4):249–55. <https://doi.org/10.5582/irdr.2017.01057>.
- [60] Castoldi F, Hyvönen MT, Durand S, et al. Chemical activation of SAT1 corrects diet-induced metabolic syndrome. *Cell Death Differ* Oct 2020;27(10):2904–20. <https://doi.org/10.1038/s41418-020-0550-z>.